A New Bcc-Fcc Orientation Relationship Observed between Ferrite and Austenite in Solidification Structures of Steels

T.J. HEADLEY and J.A. BROOKS

A new crystallographic orientation relationship (OR) between delta-ferrite and austenite has been observed in solidification microstructures of 304L and 309S austenitic stainless steels and a ternary Fe-Cr-Ni alloy. Evidence for the new OR was obtained from electron diffraction patterns in transmission electron microscopy (TEM). This relationship, $(111)_{fcc}//(110)_{bcc}$ and $[\bar{1}10]_{fcc}//[\bar{1}10]_{bcc}$, has not been previously reported for bcc-fcc systems. The $\langle 110\rangle_{fcc}//\langle 110\rangle_{bcc}$ alignment is distinctive among known bcc-fcc ORs. The new OR is related to the Kurdjumov–Sachs (K–S) and Nishiyama–Wassermann (N–W) ORs by relative rotations of 35.26 and 30 deg, respectively, about the normal to the parallel close-packed planes. In 304L fabricated by laser-engineered net shaping (LENS), delta-ferrite with the new OR was found to coexist in the microstructure with both K–S and N–W oriented ferrite, but in separate austenite grains and with less frequent occurrence. In gas-tungsten arc (GTA) welds of 309S and the Fe-Cr-Ni alloy, the new OR was the only one observed within a few grains, whereas ferrite within other grains did not establish an apparent OR with the austenite matrix.

I. INTRODUCTION

THE crystallographic orientation relationship (OR) between two phases with different crystal structures is an important parameter affecting microstructure-property relationships in such processes as precipitation from solid solution, the martensitic transformation, epitaxial growth, and solidification. An OR between two phases is often found in solidification microstructures where the relationship is established either during solidification or during subsequent solid-state transformation on cooling. For example, the weld or cast microstructures of austenitic stainless steels frequently contain ~2 to 10 vol pct delta-ferrite (δ) in the austenite (γ) matrix. Both alloy composition and solidification/cooling conditions dictate whether or not an OR is established between delta-ferrite and austenite in the resultant two-phase microstructure. Although extensive studies have been published on the solidification and microstructural evolution in austenitic stainless steel welds and castings,[1–11] it is not always straightforward to determine when the two phases were formed, or if an OR existed between delta-ferrite and austenite, when it was established. This is due in part to the complex nature and wide range of ferrite morphologies that can exist even within a single solidification structure.[12]

The structure of delta-ferrite is bcc, and that of austenite is fcc. Historically, a small number (five) of ORs has been reported to exist between bcc and fcc lattices. The three best known are the Bain,[13] the Kurdjumov and Sachs (K–S),[14] and the Nishiyama and Wasserman (N–W)[15,16] ORs. The Greninger and Troiano (G–T)[17] and the Pitsch[18] ORs are less well known. It is common practice to describe an OR by a set of planes that are parallel in the two lattices and a set of directions within those planes that are parallel. This information is given in Table I for the five known bcc-fcc ORs.

The Bain OR was proposed first in 1924 to explain the martensite* transformation in carbon steels in terms of a simple set of orthogonal strains that would transform the austenite lattice directly to the martensite lattice. It is now well known that the Bain distortion alone is not sufficient to describe the martensitic transformation in carbon steels,[19] and the Bain OR is not observed for martensite in these alloys. The Bain OR has been observed for ordered Fe_3Pt martensites and Fe_3Al-C martensite in high-aluminum steel.[20] It has not been reported for ferrite-austenite microstructures in steels, however. The K–S and N–W ORs are the most frequently reported relationships for bcc-fcc systems, including martensites in steels, and they are the only ones that have been reported for ferrite-austenite microstructures. These two relationships differ from each other by a small relative rotation of 5.26 deg. The G–T OR was reported for martensite in steel containing 0.8 pct C and 22 pct Ni. It lies approximately midway between the K–S and N–W ORs, being rotated 2.5 deg from the N–W OR. The Pitsch OR was observed for martensite formed in thin foils of an iron-nitrogen alloy, which are not subject to bulk lattice constraints as are martensites that form in bulk with the K–S or N–W OR. Neither the G–T nor Pitsch OR has been reported for ferrite-austenite microstructures. In summary, only five different ORs have been reported previously for bcc-fcc systems. Of these, the K–S and N–W ORs are the most frequently encountered and are the only ones that have been reported for ferrite-austenite microstructures.

While investigating solidification microstructures in 304L stainless steel fabricated by laser-engineered net shaping (LENS)[21] and gas-tungsten arc (GTA) welds in 309S stainless steel and a ternary Fe-Cr-Ni alloy, we observed a new OR between delta-ferrite and austenite within some grains. Evidence for this new OR was obtained from selected-area

*Martensite, with a small tetragonal distortion, is found experimentally to obey the same ORs as bcc lattices and is grouped with the bcc system in this description.

T.J. HEADLEY, Distinguished Member of Technical Staff, is with the Materials Characterization Department, Sandia National Laboratories, Albuquerque, NM 87185-1411. J.A. BROOKS, Principal Member of Technical Staff, is with the Engineered Materials Department, Sandia National Laboratories, Livermore, CA 94551-9402.

Manuscript submitted July 10, 2001.

Table I. Summary of Known Bcc-Fcc Orientation Relationships

Name	Orientation Relationship	Close-Packed Components Parallel	Minimum Angle between $\langle 110\rangle_{fcc}$ and $\langle 110\rangle_{bcc}$
Bain	$(010)_{fcc}//(010)_{bcc}$, $[001]_{fcc}//[101]_{bcc}$, $[100]_{fcc}//[10\bar{1}]_{bcc}$ $[101]_{fcc}//[100]_{bcc}$, $[\bar{1}01]_{fcc}//[001]_{bcc}$,	none	45 deg
K–S	$(111)_{fcc}//(110)_{bcc}$, $[\bar{1}10]_{fcc}//[\bar{1}11]_{bcc}$, $[11\bar{2}]_{fcc}//[\bar{1}12]_{bcc}$,	cp planes cp directions	24.74 deg
N–W	$(111)_{fcc}//(110)_{bcc}$, $[\bar{1}01]_{fcc}//[001]_{bcc}$, $[\bar{1}2\bar{1}]_{fcc}//[\bar{1}10]_{bcc}$	cp planes	25.02 deg
G–T	$(111)_{fcc}$ ~1 deg from $(110)_{bcc}$, $\langle 112\rangle_{fcc}$ ~2 deg from $[1\bar{1}0]_{bcc}$	~cp planes	~25 deg
Pitsch	$(001)_{fcc}//(101)_{bcc}$, $[\bar{1}10]_{fcc}//[\bar{1}11]_{bcc}$, $[110]_{fcc}//[12\bar{1}]_{bcc}$	cp directions	25.02 deg

Table II. Alloy Compositions (Weight Percent)

Alloy/Process	Heat	Cr	Ni	Mn	Si	C	N	P + S	Fe
304L/LENS	2	19.7	11.9	1.74	0.59	0.04	—	—	bal
309S/GTA weld	4A	25.1	14.0	1.56	0.73	0.05	~.02	0.92	bal
Fe-Cr-Ni/GTA weld	8342	18.67	11.34	—	0.008	0.009	0.003	—	bal

electron diffraction (SAED) patterns in transmission electron microscopy (TEM). This new OR has not been previously reported for bcc-fcc lattices, *i.e.*, it is not one of the five known ORs listed in Table I. We report here experimental evidence for the new OR and the experimental conditions for which we have observed it.

II. EXPERIMENTAL

The new OR was observed in solidification microstructures of two austenitic stainless steels (types 304L and 309S) and a ternary Fe-Cr-Ni alloy. Heat compositions for the three alloys are given in Table II. The solidification structures were produced by LENS fabrication of the 304L alloy and by GTA welding of the 309S and Fe-Cr-Ni alloys. In the LENS process, three-dimensional engineering components are fabricated using lasers to melt fine metal particles. In LENS fabrication of the 304L alloy, metal particles were fed into a molten pool formed by a 1 kW continuous yttrium garnet (YAG) laser. The sample was fabricated into a block 76-mm long and 9.5-mm wide using alternating layers, each comprised of overlapping passes with ~0.4 mm spacing. The passes were made with a laser power of 700 W, travel speed of 40 mm/s, and powder feed rate of 0.33 g/s. The alternating layers were deposited with a 90-deg rotation between layers. The height of each layer was approximately 0.25 mm. The 309S alloy, in the form of a 0.25 mm sheet, was GTA welded at 10.6 mm/s with 17 A, 15 V, and argon shielding. The ternary Fe-Cr-Ni alloy, in the form of a 9.5 mm plate was also GTA welded, but weld parameters were unavailable.

Thin foils for TEM analysis were prepared by electropolishing in a solution of 5 pct perchloric acid in methanol at −25 °C, with an applied potential of 18 V. Some foils were Ar ion milled following electropolishing to increase the amount of thin area for observation, or to thin a specific grain or ferrite particle within a grain sufficiently for electron-diffraction analysis. The TEM analyses were performed on a PHILIPS*-CM30 TEM at 300 kV and a JEOL**-2000FX TEM at 200 kV, using standard imaging and SAED techniques.

*PHILIPS is a trademark of the FEI Co., Hillsboro, OR.
**JEOL is a trademark of Japan Electron Optics Ltd., Tokyo.

III. RESULTS

A. *The 304L LENS Block*

We first observed ferrite with the new OR within several austenite grains in the microstructure of the 304L LENS-fabricated block. Figure 1(a) shows the optical microstructure of this block at low magnification, where the individual passes within different layers are clearly visible. Multiple-pass fabrication caused some regions within the microstructure to be melted and solidified more than once. Figure 1(b) shows an interpass boundary region at higher magnification, where the direction of solidification within the two passes is perpendicular. In this region, ferrite is confined to the center of dendrite cores, where the solidification mode would appear to be the ferrite-austenite mode (F/A mode),[2,3,5,12,13] which is solidification of primary ferrite and secondary austenite through either a eutectic or peritectic reaction. Following solidification, austenite growth consumed most of the ferrite. In other regions, solidification apparently occurred as single-phase ferrite (F mode), followed by solid-state transformation almost entirely to austenite.

Figure 2(a) is a bright-field TEM micrograph showing directionally aligned delta-ferrite particles that exhibited the new OR within one of the austenite grains. Figure 2(b) is a dark-field image from the 002-ferrite reflection, which confirms that all ferrite within this grain has the same crystallographic orientation. The position of solidification dendrites was revealed by the electropolishing procedure. The presence of dendritic microsegregation resulted in different electropolishing rates at dendrite cores and boundaries, producing thickness oscillations in the thin foil. It can be seen that ferrite particles lie in dendrite cores and are aligned close to a $\langle 100\rangle_{\delta}$ direction, which is the normal fast-growth direction for bcc material in dendritic solidification.

Figures 3(a) and (b) show composite SAED patterns from one of the ferrite particles and the adjacent austenite matrix in Figure 2(a). The foil normal was close to $[010]_{\delta}$, and the sample was tilted ±45 deg about $[010]_{\delta}$ to obtain the two

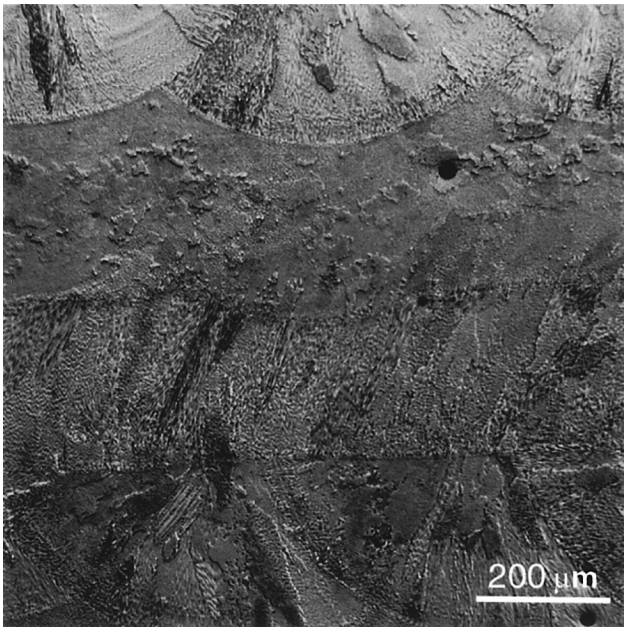

(*a*)

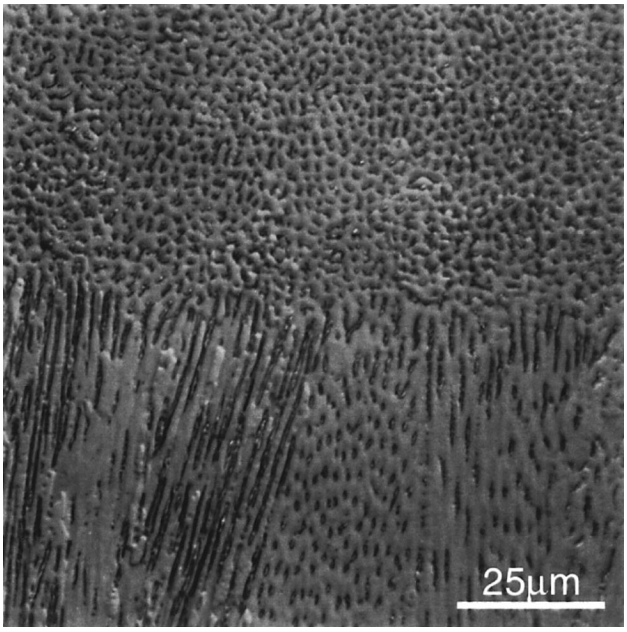

(*b*)

Fig. 1—Optical micrographs of 304L LENS-fabricated block: (*a*) low-magnification image of passes within the layers and (*b*) higher magnification image of an interpass boundary.

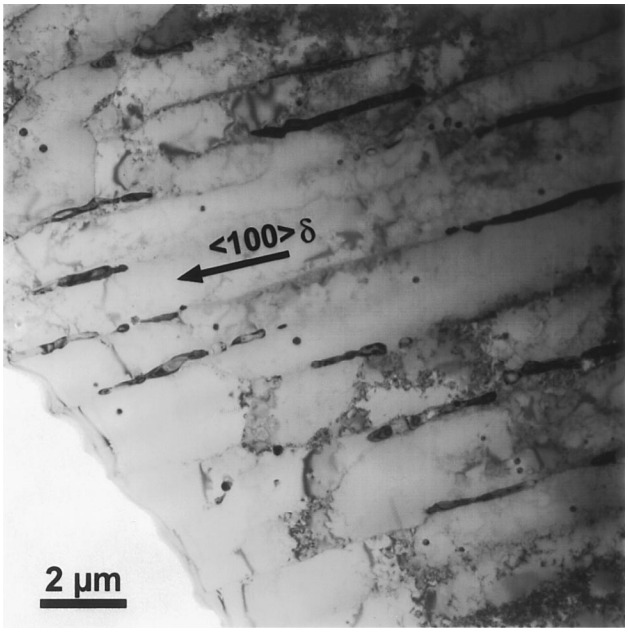

(*a*)

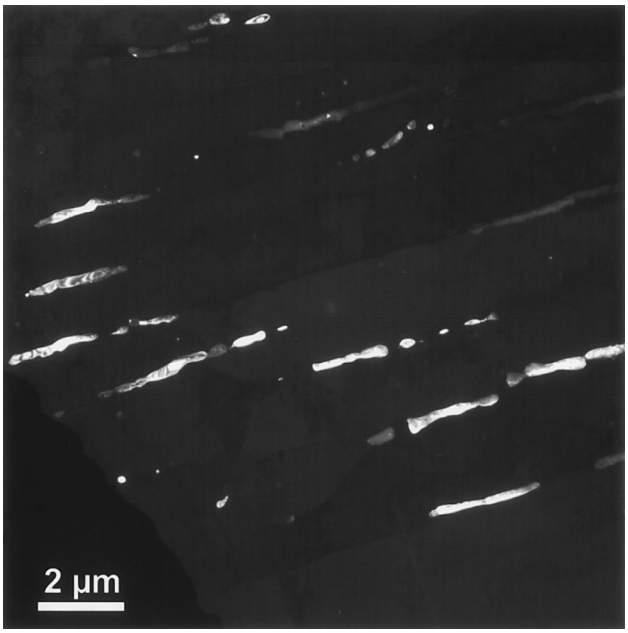

(*b*)

Fig. 2—TEM micrographs of delta-ferrite particles in dendrite cores within an austenite grain in 304L LENS-fabricated block: (*a*) bright-field image and (*b*) dark-field image from the 002-ferrite reflection.

patterns. These patterns are representative of all ferrite particles in the grain. In Figure 3(a), the $[\bar{1}10]$ zone-axis pattern of austenite and the $[\bar{1}10]$ zone-axis pattern of ferrite are superimposed, hence, the $[\bar{1}10]_\gamma$ and $[\bar{1}10]_\delta$ zone axes are parallel normal to the plane of the pattern. The 111_γ and 110_δ reflections are aligned within the pattern, indicating that the $(111)_\gamma$ planes are parallel to the $(110)_\delta$ planes. Hence, the OR within this grain is

$$(111)_\gamma // (110)_\delta \text{ and } [\bar{1}10]_\gamma // [\bar{1}10]_\delta$$

Likewise, in Figure 3(b), the $[11\underline{1}]_\gamma$ and $[\underline{1}10]_\delta$ zone-axis patterns are superimposed, and the $\bar{2}20_\gamma$ and $\bar{1}10_\delta$ reflections are aligned within the pattern, confirming the aforementioned OR. The parallel alignments in this new OR are summarized in Table III. The axis/angle pair description[22] for this new OR is $[\bar{1}10]$/35.26 deg; that is, the bcc and fcc lattices are rotated 35.26 deg (the angle between [111] and [110]) relative to each other about the common $[\bar{1}10]$ direction, as shown in Figure 4(a). Rotation through this angle would bring the two lattices into a cube-on-cube OR. The sets of coincident low-index directions (and planes, since both lattices are cubic) that result from this axis-angle alignment are given in column two in Table III and are shown on the composite stereogram in Figure 4(b).

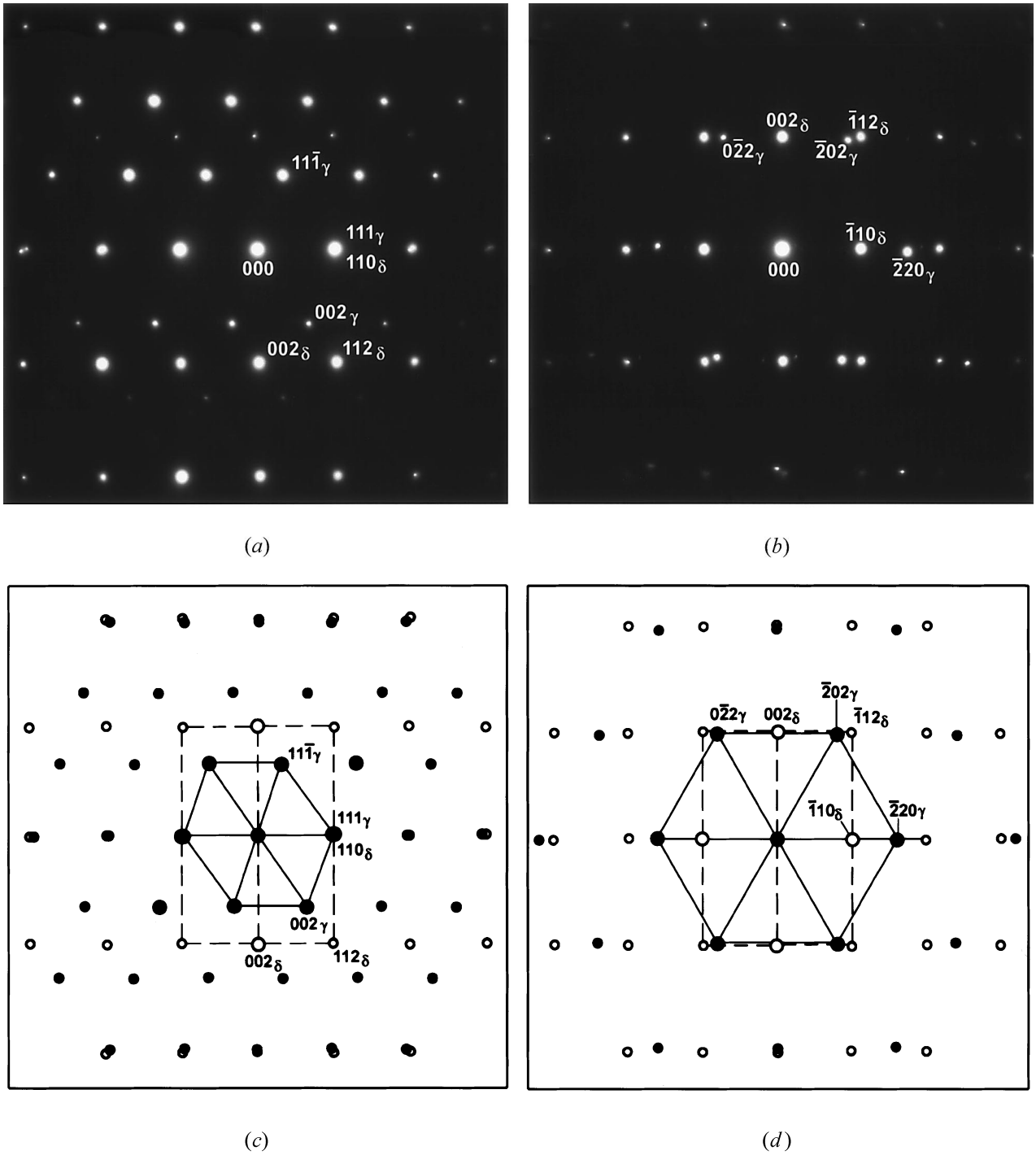

Fig. 3—SAED patterns for the grain in Fig. 2: (*a*) $[\bar{1}10]_\gamma$ and $[\bar{1}10]_\delta$ zone-axis patterns superimposed, (*b*) $[111]_\gamma$ and $[110]_\delta$ zone-axis patterns superimposed, and (*c*) and (*d*) computed patterns corresponding to (a) and (b), respectively.

Composite SAED zone-axis patterns for the new OR were computed using a lattice-parameter ratio (a_{fcc}/a_{bcc}) of 1.25, which was measured from Figure 3(a). Computed patterns corresponding to the experimental patterns in Figures 3(a) and (b) are shown in Figures 3(c) and (d), respectively. Solid and open circles correspond to austenite and ferrite reflections, respectively. Solid and dashed lines have been added to elucidate the austenite and ferrite reciprocal lattice nets. Inspection reveals a small angular difference between the experimental and computed patterns, which is due to the fact that the real OR deviates slightly from the exact OR of $(111)_\gamma//(110)_\delta$ and $[\bar{1}10]_\gamma//[\bar{1}10]_\delta$. The amount of deviation in this case was measured from the projected centers of the zone axes in Figures 3(a) and (b) and was found to be $(111)_\gamma$ and $(110)_\delta$ 0.7 deg apart and $[\bar{1}10]_\gamma$ and $[\bar{1}10]_\delta$ 1.3 deg apart.

Another austenite grain, in which the remnant delta-ferrite exhibited the new OR, was found within a second TEM foil prepared from the 304L LENS-fabricated block. This grain was tilted until the beam was aligned with the coincident set of directions $[110]_\gamma//[11\bar{1}]_\delta$ (Table III and Figure 4(b)).

Table III. Summary of Parallel Relationships in the New OR

Name	Orientation Relationship	Close-Packed Components Parallel
New OR (this study)	$(111)_{fcc}//(110)_{bcc}$, $[-110]_{fcc}//[-110]_{bcc}$ $[11\text{-}2]_{fcc}//[00\text{-}1]_{bcc}$	cp planes
	$[110]_{fcc}//[11\text{-}1]_{bcc}$ $[001]_{fcc}//[112]_{bcc}$ $[112]_{fcc}//[221]_{bcc}$ $[22\text{-}1]_{fcc}//[11\text{-}2]_{bcc}$	cp directions (not in the parallel cp planes)

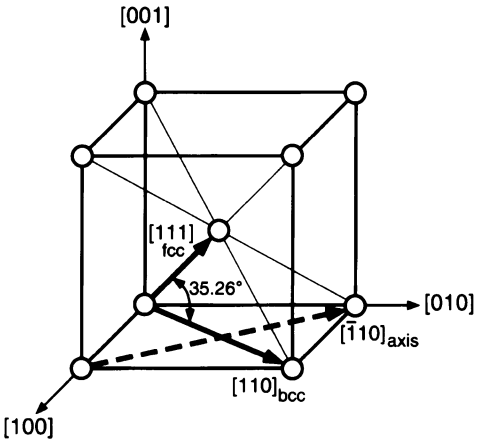

(*a*)

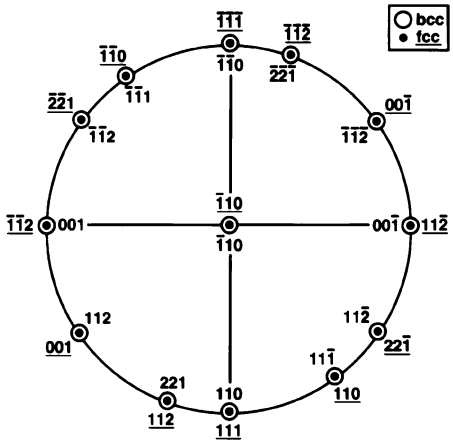

(*b*)

Fig. 4—(*a*) Axis-angle diagram showing the 35.26 deg rotation between $[111]_{fcc}$ and $[110]_{bcc}$ about the common $[\bar{1}10]$ direction that produces the new OR. (*b*) Composite stereogram showing the sets of coincident low-index directions generated by the new OR. Indices of fcc poles are underlined.

The resulting experimental and computed diffraction patterns are shown in Figures 5(a) and (b). Here, the $[110]_\gamma$ and $[11\bar{1}]_\delta$ zone-axis patterns are superimposed, confirming that $[\bar{1}10]_\gamma//[11\bar{1}]_\delta$ are normal to the pattern, while the $\bar{2}20_\gamma$ and $\bar{1}10_\delta$ reflections were approximately aligned within the pattern. For this grain, the deviation from the exact OR is $[110]_\gamma$ and $[11\bar{1}]_\delta$ 1.8 deg apart and $(\bar{1}10)_\gamma$ and $(\bar{1}10)_\delta$ 5 deg apart. This deviation is larger than that measured for the grain in Figures 2 and 3.

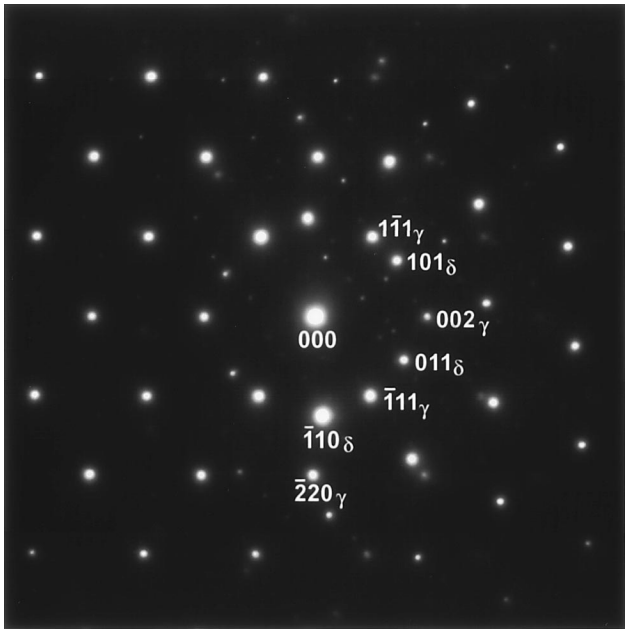

(*a*)

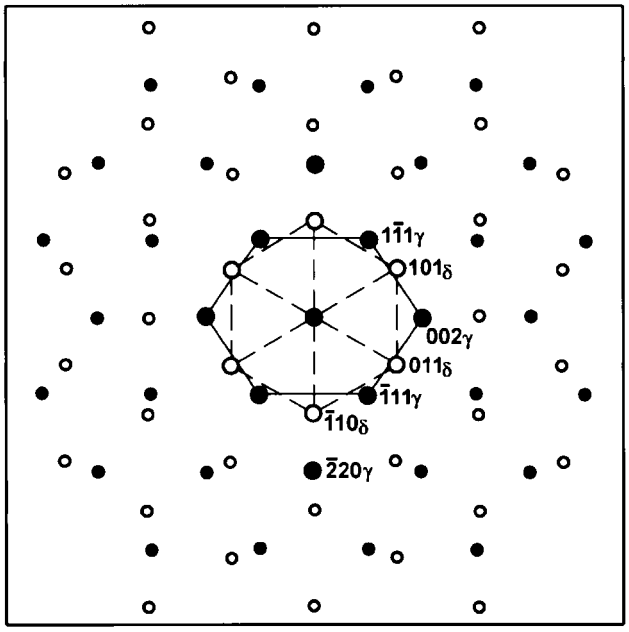

(*b*)

Fig. 5—(*a*) SAED pattern for a second grain exhibiting the new OR in 304L LENS-fabricated block, $[110]_\gamma$ and $[111]_\delta$ zone-axis patterns superimposed. Weak spots in the background arise from diffraction effects at the interface. (*b*) Computed pattern corresponding to (a).

These two grains were the only ones found exhibiting the new OR among all grains in the thin portions of the two TEM foils from this material. In all other grains, remnant delta-ferrite resided in dendrite cores and exhibited either the K–S or N–W OR. No grains were found in which the ferrite did not have an OR with the austenite matrix.

B. *The 309S GTA Weld*

Figure 6(a) is an optical micrograph of the single-pass, autogenous GTA weld in the alloy 309S sheet metal. Here,

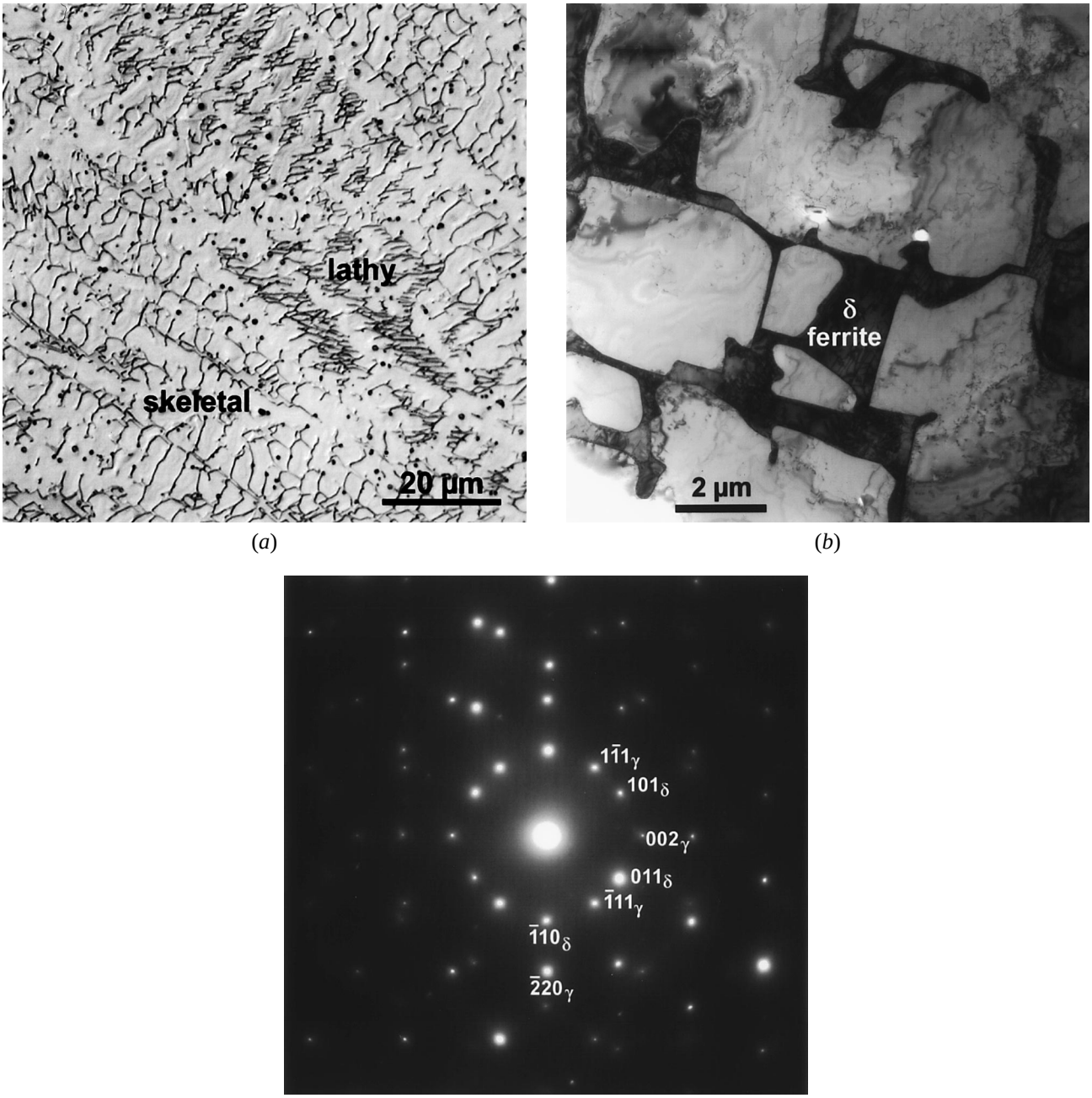

(*a*) (*b*)

(*c*)

Fig. 6—(*a*) Optical micrograph of single-pass autogenous GTA weld in 309S sheet, (*b*) TEM micrograph of delta-ferrite with skeletal morphology, and (*c*) SAED pattern for (b), $[110]_\gamma$ and $[111]_\delta$ zone-axis patterns superimposed.

the microstructure results from a single solidification and cooling event, unlike the multiple-pass microstructure of the 304L LENS-fabricated block. Figure 6(a) contains some regions where delta-ferrite has a classical skeletal (or vermicular) morphology with secondary branching and other regions where it has a lathy morphology. Tin quenching of welds in this material showed that solidification occurred by the F/A mode, in which any OR would have been established during solidification. Figure 6(b) is a TEM micrograph of a grain in which all the delta-ferrite had a more skeletal-appearing morphology and exhibited the new OR with the austenite matrix. The experimental diffraction pattern for ferrite/austenite in this grain is shown in Figure 6(c) and is similar to the pattern in Figure 5(a). The $[110]_\gamma$ and $[1\bar{1}\bar{1}]_\delta$ zone-axis patterns are superimposed, and the $\bar{2}20_\gamma$ and $\bar{1}10_\delta$ reflections are nearly aligned within the pattern. The deviation from the exact OR is $[110]_\gamma$ and $[1\bar{1}\bar{1}]_\delta$ 3.5 deg apart normal to the pattern and $[\bar{1}10]_\gamma$ and $[\bar{1}10]_\delta$ 1 deg apart in the plane of the pattern. The ferrite in several other grains, which were thin enough to analyze in this foil, did not have an established OR with the austenite matrix. No grains were found containing K–S or N–W oriented ferrite within the thin region of the foil.

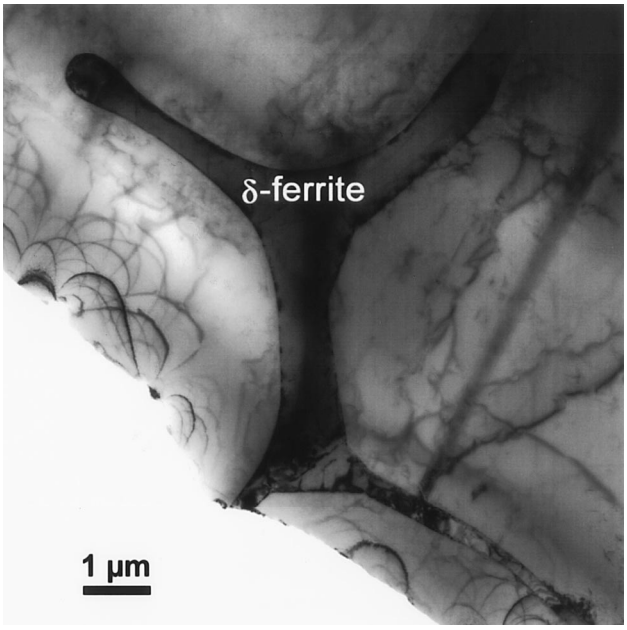

(*a*)

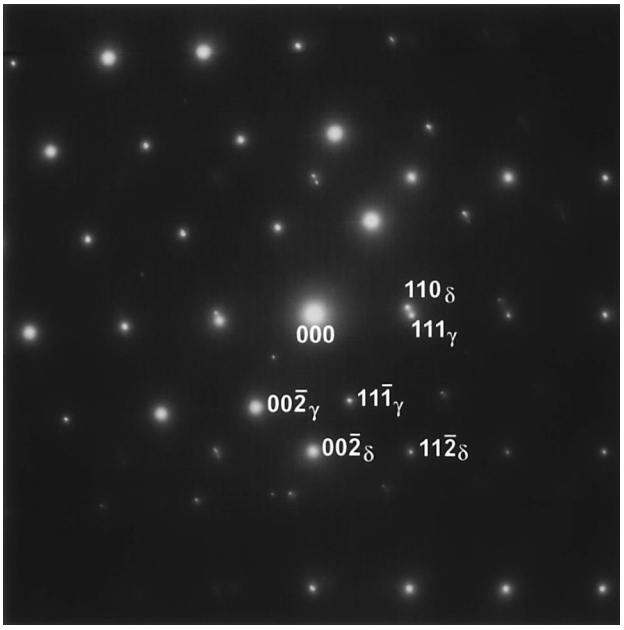

(*b*)

Fig. 7—(*a*) TEM micrograph of skeletal delta-ferrite in single-pass autogenous GTA weld in Fe-Cr-Ni alloy plate and (*b*) SAED pattern for (a), $[1\bar{1}0]_\gamma$ and $[1\bar{1}0]_\delta$ zone-axis patterns superimposed.

C. *The Fe-Cr-Ni alloy GTA Weld*

Figure 7(a) is a TEM micrograph of the single-pass, autogeneous GTA weld in the ternary Fe-Cr-Ni alloy, showing delta-ferrite with a classical skeletal (or vermicular) morphology in the austenite matrix. All ferrite within this grain had a skeletal morphology with secondary branching and exhibited the new OR with the surrounding austenite. The solidification sequence for this grain is not certain, but this ferrite morphology is most often associated with the F/A solidification mode.[1] The experimental diffraction pattern from this ferrite and adjacent austenite is shown in Figure 7(b), confirming the new OR. The pattern is similar to that in Figure 3(a), but viewed from the opposite direction, *i.e.*, along $[1\bar{1}0]_\gamma$ and $[1\bar{1}0]_\delta$. (An alternate interpretation is that Figures 3(a) and 7(b) show two different variants of the new OR, where $(111)_\gamma//(110)_\delta$ are shown in Figure 3(a) and $(11\text{-}1)_\gamma//(110)_\delta$ are shown in Figure 7(b).) From Figure 7(b), the deviation from the exact OR was measured to be $[1\text{-}10]_\gamma$ and $[1\bar{1}0]_\delta$ 2 deg apart normal to the pattern and $[111]_\gamma$ and $[110]_\delta$ 3.5 deg apart in the plane of the pattern. This is a larger deviation than that for the grain in Figure 3(a). As in the 309S GTA weld, this was the only grain found within the thin area of the foil in which the ferrite/austenite had established an OR. The ferrite in other grains examined did not appear to have an OR with the austenite matrix.

IV. DISCUSSION

A. *Distinction from other ORs*

It can be seen from column two in Tables I and III that the new OR is the only one that aligns a $\langle 110\rangle_{fcc}$ direction parallel to a $\langle 110\rangle_{bcc}$ direction. This condition is not approached in any of the other bcc-fcc ORs. Column four in Table I lists the minimum angular separation between the $\langle 110\rangle_{fcc}$ and $\langle 110\rangle_{bcc}$ directions. It can be seen that the $\langle 110\rangle$ directions in the other ORs come no closer than ~25 deg to alignment. This fact can be verified from inspection of composite stereograms with poles plotted for the various ORs. This $\langle 110\rangle_{fcc}//\langle 110\rangle_{bcc}$ alignment provided a distinctive fingerprint in electron diffraction for distinguishing ferrite/austenite structures that had the new OR from other possible ORs. The $\langle 110\rangle_{fcc}$ and $\langle 110\rangle_{bcc}$ zone-axis patterns in electron diffraction are familiar, and their superposition (*e.g.*, Figure 3(a)) will be readily recognized when encountered in the diffraction pattern of fcc-bcc lattices with the new OR. The three different patterns in Figures 3(a), 3(b), and 5(a) or 6(c) contain this $\langle 110\rangle_{fcc}//\langle 110\rangle_{bcc}$ component either normal to or within the plane of the pattern and are the most diagnostic for identifying bcc-fcc structures that have the new OR. They are not similar to any patterns of superimposed low-index zones that occur in the other bcc-fcc ORs.

In a related matter, other investigators[2,3,6,11] have frequently noted a close alignment (<10 deg) between the $\langle 100\rangle$ directions of ferrite and austenite in solidification microstructures of stainless steels. Such alignment rules out the presence of ferrite with the new OR, for which the minimum angular separation between the $\langle 100\rangle_{fcc}$ and $\langle 100\rangle_{bcc}$ directions is 24.74 deg.

B. *Relation to the K–S and N–W ORs*

Two phases with different crystal symmetry will often adopt an OR between them, where close-packed planes in each phase are parallel. Column three in Tables I and III lists the close-packed components that are parallel in the various bcc-fcc ORs. It can be seen that close-packed planes are parallel in the K–S, N–W, and new ORs. Only the K–S OR also aligns close-packed directions within those planes. The new OR does align a pair of close-packed directions,

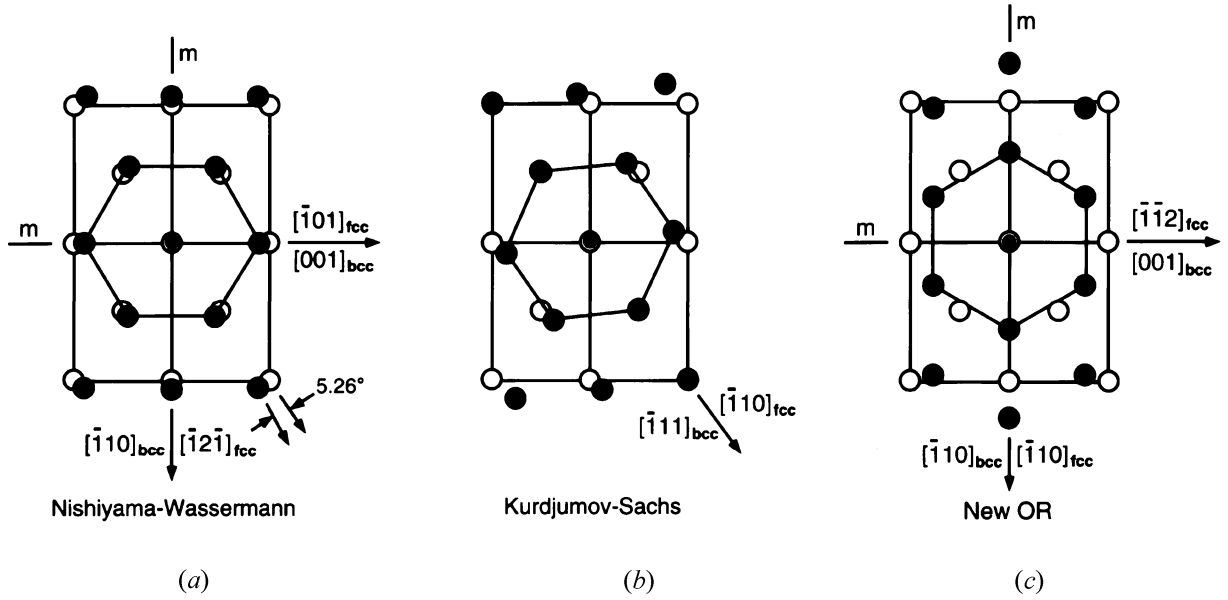

Fig. 8—Atomic arrangement in close-packed planes for bcc (open circle) and fcc (solid circle) lattices as they are superimposed in (*a*) N–W OR, (*b*) K–S OR, and (*c*) the new OR. In (a) and (c), *m* denotes the position of mirror planes in the 2-D pattern symmetry, while arrows and indices denote real-lattice directions normal to the mirror planes ((a) and (b) from Dahmen[23]).

$[110]_{fcc}//[11\bar{1}]_{bcc}$, but they do not lie in the parallel close-packed planes, $(111)_\gamma//(110)_\delta$.

Dahmen[23] has elucidated the rotations relating the Bain, N–W, K–S, G–T, and Pitsch ORs to one another. Here, we utilize his graphical approach to show the rotations relating the new OR to the K–S and N–W ORs, each of which has a set of parallel close-packed planes. Figure 8 shows the atomic arrangements in the close-packed planes superimposed as they are aligned in the three ORs. Open and solid circles depict atoms in the $\{110\}_{bcc}$ and $\{111\}_{fcc}$ planes, respectively. Lines forming rectangles and hexagons show the twofold and sixfold rotational symmetry of the individual two-dimensional nets. Figure 8(a) shows the atomic alignment for the N–W OR. The two-dimensional symmetry of the combined nets is mm2. One mirror plane is normal to $[001]_{bcc}//[\bar{1}01]_{fcc}$ and the other is normal to $[\bar{1}10]_{bcc}//[\bar{1}2\bar{1}]_{fcc}$. The close-packed directions are misaligned by 5.26 deg. A relative rotation of one lattice through 5.26 deg about the normal brings one set of close-packed directions into alignment, as shown in Figure 8(b). This is the atomic alignment for the K–S OR. The two-dimensional symmetry of the overall pattern is lower, as it no longer contains mirror planes. Figure 8(c) shows the alignment for the new OR. In this case, the overall pattern symmetry once again is mm2. One mirror plane is normal to $[001]_{bcc}//[\bar{1}\bar{1}2]_{fcc}$ and the other is normal to $[\bar{1}10]_{bcc}//[\bar{1}10]_{fcc}$. Thus, alignment of the $[\bar{1}10]_{bcc}$ and $[\bar{1}10]_{fcc}$ directions in the new OR introduces mirror-plane symmetry into the atomic alignment in the close-packed planes.

Figure 9 shows composite stereograms for the three ORs projected normal to the close-packed planes and oriented to match Figure 8. Open and solid circles represent bcc and fcc poles, respectively. Indices for fcc poles are underlined. Rectangles and hexagons in the stereograms show the relative orientations of the atomic nets in Figure 8. It can be seen from Figures 9(a) and (b) that a relative rotation of 5.26 deg about the normal to the parallel closed-packed planes will bring the N–W OR into coincidence with the K–S OR, or *vice versa*. (The relative rotations relating the N–W to the Bain OR and the K–S to the Pitsch OR are also shown after Dahmen[23]). In like manner, comparing Figure 9(c) to Figures 9(a) and (b) shows that a relative rotation of either 30 or 35.26 deg about the normal to the parallel closed-packed planes will bring the new OR into coincidence with either the N–W or K–S OR, respectively. Thus, the new OR is related to the N–W and K–S ORs by relative rotations about the normal to the close-packed planes.

C. *Deviation from Exact Orientation*

The measured deviations from the exact $(111)_\gamma//(110)_\delta$ and $[\bar{1}10]_\gamma//[\bar{1}10]_\delta$ OR are tabulated in Table IV for those grains found to exhibit the new OR in this study. The range of deviation is ~1 to 5 deg. The experimental error for these measurements is estimated to be 0.5 deg. It should be noted also that the magnitude of this deviation varied up to ~1 deg with location throughout a given grain, which is typical of the amount of misorientation within a grain resulting from dendritic solidification. By comparison, both the K–S and N–W oriented ferrite in the LENS-fabricated 304L block also deviated from the exact ORs, but with a more limited range, typically <2 deg for N–W oriented ferrite and ~1 deg for K–S oriented ferrite. For example, Figure 10(a) shows the experimental diffraction pattern for ferrite oriented ~1.1 deg from the exact N–W orientation in the LENS-fabricated 304L block. Figure 10(b) is the corresponding computed pattern for the exact N–W OR.

D. *Frequency of Occurrence*

We observed a total of four grains exhibiting the new OR in the three materials investigated by TEM in this study. This number represents a relatively small proportion of the total number of grains (~40) within the collective thin area

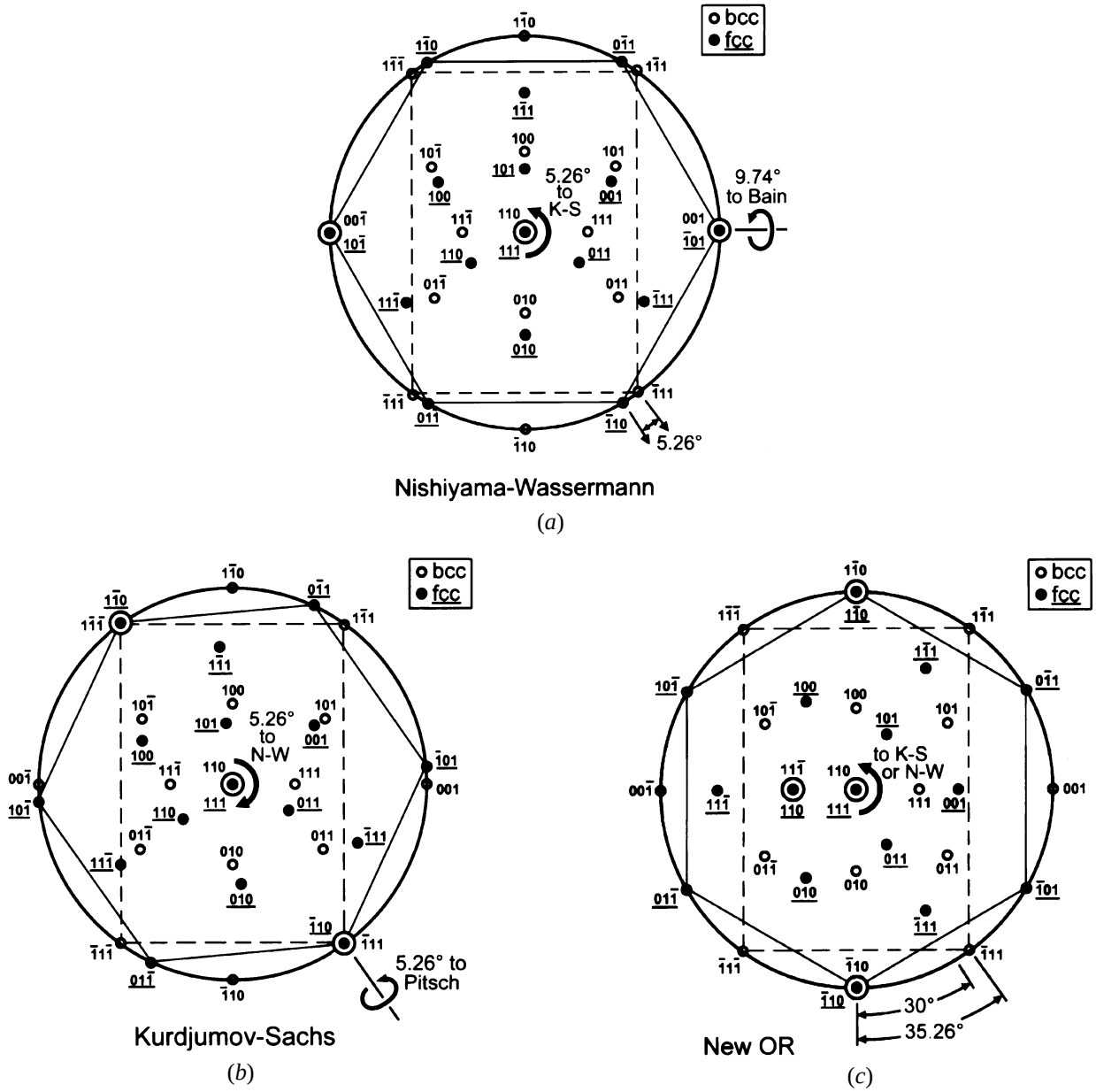

Fig. 9—Composite stereograms projected normal to the parallel close-packed planes for (*a*) N–W OR, (*b*) K–S OR, and (*c*) the new OR, oriented to match Fig. 8. Open and solid circles represent bcc and fcc poles, respectively. Indices for fcc poles are underlined. Relative rotations about the projected normal ($[111]_{fcc}//[110]_{bcc}$) relate the three ORs to each other ((a) and (b) from Dahmen[23]).

Table IV. Measured Deviations from Exact OR

Sample	Grain	$(111)_\gamma$ and $(110)_\delta$	$[-110]_\gamma$ and $[-110]_\delta$
304L-2 Lens block	1	0.7 deg apart	1.3 deg apart
	2	1.8 deg apart	5 deg apart
309S-4A GTA weld	1	3.5 deg apart	1 deg apart
Fe-Cr-Ni GTA weld	1	3.5 deg apart	2 deg apart

of the four TEM foils examined. Therefore, one must consider if the orientations within these four grains resulted merely from coincidental alignment. First, we consider an infinite number of grains having a *completely* random set of coincidental orientations between ferrite and austenite. This set contains only a very small subset (~0.3 pct) whose orientations lie within the ±5-deg range of deviation from the exact new OR that was observed in this study. It is highly unlikely that we would have encountered as many as four grains out of 40 with this orientation if they were a result of random alignment. Second, a more restricted case of coincidental alignment should be considered. Inoue *et al.*[6] recently reported in certain austenitic stainless steel welds that, depending on the welding heat-source direction, some ferrite established a K–S OR, other ferrite established only a parallel relationship between the ⟨100⟩ directions with austenite, and still other ferrite established only a parallel relationship between close-packed planes with austenite. We consider the latter case, where a set of close-packed planes is parallel between the two lattices, but the relative orientation

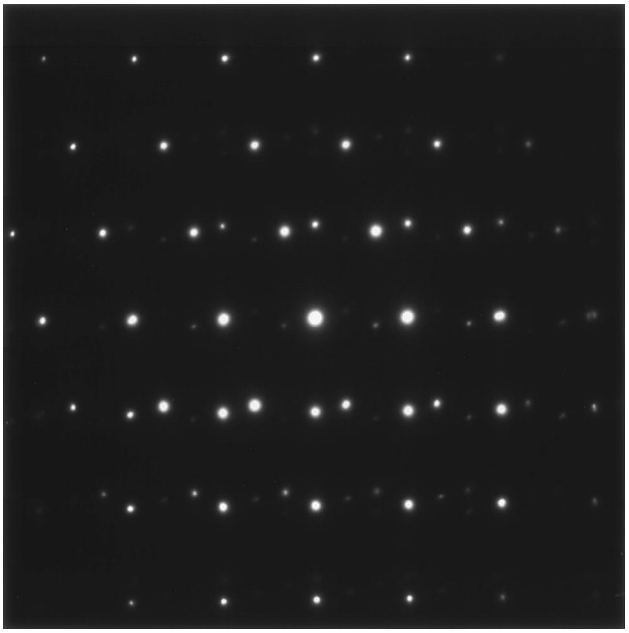

(*a*)

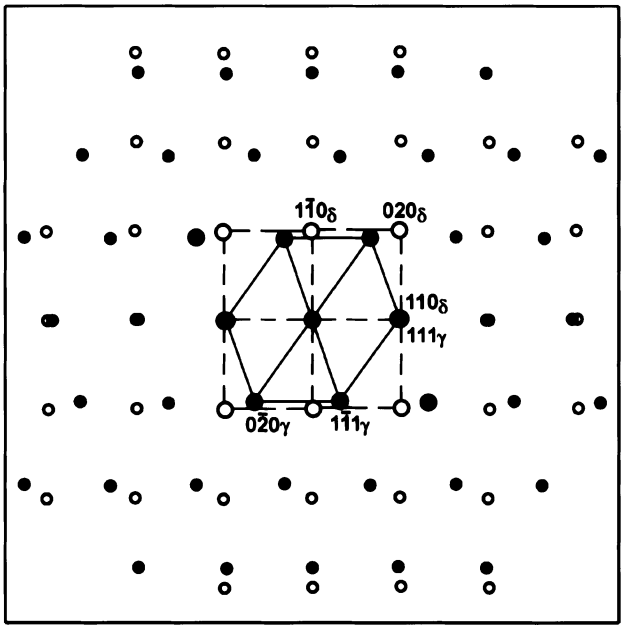

(*b*)

Fig. 10—(*a*) SAED pattern for a grain containing N–W oriented delta-ferrite in 304L LENS-fabricated block, $[\bar{1}01]_\gamma$ and $[001]_\delta$ zone-axis patterns superimposed, and (*b*) computed pattern corresponding to (a). Extra spots in (a) arise from double diffraction.

within those planes may be random. Then, the subset of chance grains whose orientations lie within the ±5-deg range of deviation from the exact new OR is the ratio of 20 to 360 deg, or about one grain in 18. (We double the ±5-deg range in this ratio because the diffraction patterns for positive and negative zone axes will appear to give the same OR). In the present case of the 304L LENS-fabricated block, most grains contained either K–S or N–W oriented ferrite. The only exceptions were the two grains with the new OR. This result is inconsistent with the chance alignment of one grain in 18. We conclude that the occurrences of the new OR found in this study were not coincidental alignments.

E. *Formation of the new OR*

Our evidence suggests that the new OR observed between delta-ferrite and austenite in this study was established during solidification rather than in the solid state. The structures examined here solidified largely in the F/A mode, where a large fraction of the liquid solidifies as primary ferrite followed by secondary solidification of the remaining liquid as austenite. The 309S GTA weld was shown through tin quenching to solidify in the F/A mode, apparently by a peritectic reaction. The Fe-Cr-Ni alloy GTA weld appeared in optical microscopy to have solidified in mixed mode, with most grains solidifying in the F/A mode but with others solidifying in the A/F mode (as primary austenite with secondary ferrite). Although the LENS-fabricated 304L material underwent multiple fusion and solidification events during sequential passes, detailed scanning TEM profiles, revealing the nature of dendritic microsegregation and ferrite confined totally to dendrite cores, indicated that most regions of this sample also solidified in the F/A mode during the final pass.

Thus most, if not all, of the structures that exhibited the new OR in this study were formed during F/A-mode solidification. The new OR would then be established *during* solidification, as secondary austenite nucleates on primary ferrite. In this case, it is likely that the bulk strain energy would be minimal or nonexistent, and nucleation would be controlled primarily by the volume and interfacial energies. This may be, in part, why the new OR has not been observed for solid-state crystallographic transformations in which the strain-energy component is significant, *e.g.*, the martensitic transformation. Similarly, Clarke and Stobbs[24] suggested that the lack of accompanying strain during solidification may be why the distribution of ORs between bcc-chromium and fcc-copper phases in a unidirectionally solidified Cu-Cr eutectic alloy was not intermediate between the K–S and N–W ORs, as expected. In the absence of significant bulk strain during solidification, the magnitude of the interfacial energy may control the selection of a given OR between phases. Furthermore, since the K–S and N–W ORs occur far more frequently in F/A-solidified structures of ferrite and austenite, the interfacial energies associated with those two ORs may be somewhat lower than that for the new OR. It is not clear what role, if any, subsequent growth may play on the final statistical distribution. Computational simulations of the interfacial energies for these three ORs would add further insight as to their statistical occurrence during solidification. Similarly, computational studies would add insight as to whether the new OR could be established in solid-state transformation at high temperatures, where the bulk strain-energy component may be reduced.

V. CONCLUSIONS

A TEM investigation of solidification microstructures in LENS-fabricated 304L stainless steel and GTA welds in 309S stainless steel and a ternary Fe-Cr-Ni alloy led to the observation of a new OR between delta-ferrite and austenite within some grains. Evidence for this new OR was obtained

from SAED patterns. This new OR has not been previously reported for bcc-fcc systems. The following conclusions can be drawn from this work.

1. The new OR is $(111)_{fcc}//(110)_{bcc}$ and $[\bar{1}10]_{fcc}//[\bar{1}\bar{1}0]_{bcc}$. The $\langle 110\rangle_{fcc}//\langle 110\rangle_{bcc}$ alignment is distinctive among known bcc-fcc ORs. This fact that may be utilized in electron diffraction analysis to distinguish the new OR from other known ORs in bcc-fcc microstructures. The diagnostic zone-axis patterns are $[\bar{1}10]_{fcc}//[\bar{1}\bar{1}0]_{bcc}$, $[111]_{fcc}//[110]_{bcc}$, and $[110]_{fcc}//[11\bar{1}]_{bcc}$.
2. A set of close-packed planes is parallel between the bcc and fcc lattices in the new OR, but the close-packed directions are not parallel. Since the close-packed planes are parallel, the new OR is related to the well-known K–S and N–W ORs by relative rotations about the normal to the parallel close-packed planes. Rotations of 35.26 and 30 deg bring the new OR into coincidence with the K–S and N–W ORs, respectively.
3. The frequency of occurrence of ferrite/austenite with this new OR was quite low for the steel compositions and specific solidification/cooling conditions investigated in this study. It was observed in a total of two grains in the LENS-fabricated 304L stainless steel and in one grain each in the GTA welds of 309S stainless steel and the ternary Fe-Cr-Ni alloy.
4. The new OR observed in this study is believed to have been established during F/A-mode solidification, where the bulk strain energy during nucleation of secondary austenite on primary ferrite is likely to be minimal. The relative magnitude of the interfacial energy is then suggested to be controlling the selection of a given OR between the two phases and, hence, has a major influence on the statistical distribution of ORs observed in the solidified microstructures.

ACKNOWLEDGMENTS

The authors thank Drs. U. Dahmen and J.R. Michael for helpful discussions. Sandia is a multiprogram laboratory operated by Sandia Corporation, a Lockheed Martin Company, for the United States Department of Energy under Contract No. DE-AC04-94AL85000.

REFERENCES

1. J.A. Brooks and A.W. Thompson: *Int. Mater. Rev.*, 1991, vol. 36, pp. 16-44.
2. J.A. Brooks, J.C. Williams, and A.W. Thompson: *Proc. Conf. on Trends in Welding Research in the United States*, S.A. David, ed., ASM INTERNATIONAL, Metals Park, OH, 1981, pp. 331-57.
3. J.A. Brooks, J.C. Williams, and A.W. Thompson: *Metall. Trans. A*, 1983, vol. 14A, pp. 1271-81.
4. J.A. Brooks, N.C.Y. Yang, and J.S. Krafcik: *Proc. Conf. on Trends in Welding Research in the United States*, S.A. David, ed., ASM INTERNATIONAL, Metals Park, OH, 1992, pp. 173-80.
5. J.A. Brooks, A.W. Thompson, and J.C. Williams: *Weld. J. Res. Suppl.*, 1984, vol. 63, pp. 71s-83s.
6. H. Inoue, T. Koseki, S. Ohkita, and M. Fuji: *Sci. Technol. Weld. Joining*, 2000, vol. 5, pp. 385-96.
7. H. Inoue, T. Koseki, S. Ohkita, and M. Fuji: *Weld. Int.*, 1997, vol. 11, pp. 937-49.
8. H. Inoue, T. Koseki, S. Ohkita, and M. Fuji: *Weld. Int.*, 1998, vol. 15, pp. 282-96.
9. N. Suutala, T. Takalo, and T. Mosio: *Metall. Trans. A*, 1979, vol. 10A, pp. 512-14.
10. N. Suutala, T. Takalo, and T. Mosio: *Metall. Trans. A*, 1979, vol. 10A, pp. 1173-81.
11. N. Suutala, T. Takalo, and T. Mosio: *Metall. Trans. A*, 1980, vol. 11A, pp. 717-25.
12. S.A. David: *Weld. J. Res. Suppl.*, 1981, vol. 60, pp. 633s-671s.
13. E. Bain: *Trans. TMS-AIME*, 1924, vol. 70, pp. 25-46.
14. G. Kurdjumov and G. Sachs: *Z. Phys.*, 1930, vol. 64, pp. 325-43.
15. Z. Nishiyama: *Sci. Rep. Res. Inst., Tohoku Univ.*, 1934, vol. 23, pp. 637-64.
16. G. Wasserman: *Arch. Eisenhuttenwes.*, 1933, vol. 16, p. 647.
17. A.B. Greninger and A.R. Troiano: *Trans. TMS-AIME*, 1949, vol. 185, pp. 590-98.
18. W. Pitsch: *Phil. Mag.*, 1959, vol. 4, pp. 577-84.
19. C.S. Barrett and T.B. Massalski: *Structure of Metals*, 3rd ed., McGraw-Hill Book Co., New York, NY, 1966, pp. 520-25.
20. K. Shimizu and Z. Nishiyama: *Metall. Trans.*, 1972, vol. 3, pp. 1055-68.
21. M.I. Griffith, D.M. Keicher, C.L. Atwood, C.L. Romero, J.E. Smugeresky, L.D. Harwell, and L.D. Green: *Proc. Symp. on Solid Freeform Fabrication*, University of Texas Publishers, Austin, TX, 1996, p. 125.
22. J.W. Edington: *Practical Electron Microscopy in Materials Science*, Van Nostrand Reinhold Co., New York, NY, 1976, pp. 68-72.
23. U. Dahmen: *Acta Metall.*, 1982, vol. 30, pp. 63-73.
24. D.R. Clarke and W.M. Stobbs: *Met. Sci.*, 1974, vol. 8, pp. 242-46.